Available online at www.sciencedirect.com
ScienceDirect
International Journal of Solids and Structures 45 (2008) 2613–2628
INTERNATIONAL JOURNAL OF SOLIDS AND STRUCTURES
www.elsevier.com/locate/ijsolstr

On constructing the analytical solutions for localizations in a slender cylinder composed of an incompressible hyperelastic material

Hui-Hui Dai [a,*], Yanhong Hao [b], Zhen Chen [c]

[a] Department of Mathematics and Liu Bie Ju Centre for Mathematical Sciences, City University of Hong Kong, 83 TatChee Avenue, Kowloon Tong, Hong Kong
[b] Department of Mathematics, City University of Hong Kong, 83 TatChee Avenue, Kowloon Tong, Hong Kong
[c] Department of Civil and Environmental Engineering, University of Missouri-Columbia, Columbia, MO 65211-2200, USA

Received 7 August 2007; received in revised form 21 November 2007
Available online 28 December 2007

Abstract

In this paper, we study the localization phenomena in a slender cylinder composed of an incompressible hyperelastic material subjected to axial tension. We aim to construct the analytical solutions based on a three-dimensional setting and use the analytical results to describe the key features observed in the experiments by others. Using a novel approach of coupled series-asymptotic expansions, we derive the normal form equation of the original governing nonlinear partial differential equations. By writing the normal form equation into a first-order dynamical system and with the help of the phase plane, we manage to solve two boundary-value problems analytically. The explicit solution expressions (in terms of integrals) are obtained. By analyzing the solutions, we find that the width of the localization zone depends on the material parameters but remains almost unchanged for the same material in the post-peak region. Also, it is found that when the radius–length ratio is relatively small there is a snap-back phenomenon. These results are well in agreement with the experimental observations. Through an energy analysis, we also deduce the preferred configuration and give a prediction when a snap-through can happen. Finally, based on the maximum-energy-distortion theory, an analytical criterion for the onset of material failure is provided.

Keywords: Localization; Hyperelasticity; Cylinder; Bifurcations of PDE's

1. Introduction

The field of fracture mechanics is becoming extremely broad with the occurrence of unexpected failure of weapons, buildings, bridges, ships, trains, airplanes, and various machines. There are two fundamental fracture criterions: the strain energy release rate (i.e., G Theory) and the stress intensity factor (i.e., K Theory); see

* Corresponding author. Tel.: +852 27888660; fax: +852 27888561.
E-mail address: mahhdai@cityu.edu.hk (H.-H. Dai).

0020-7683/$ - see front matter © 2007 Elsevier Ltd. All rights reserved.
doi:10.1016/j.ijsolstr.2007.12.013

Arthur and Richard (2002). The experimentally determined stress intensity depends on the specimen size, and the fracture is accompanied by energy localization and concentration.

Localization is manifested by degradation of material properties with localized large deformations, and this feature often results in formation and propagation of macrocracks through engineering structures. Due to the importance of localization phenomena in structural safety assessment, much research has been conducted to resolve experimental, theoretical and computational issues associated with localization problems, as reviewed by Chen and Schreyer (1994) and Chen and Sulsky (1995). For hyperelastic materials, important progress has been made based on the gradient approach; see Aifantis (1984) and Triantafyllidis and Aifantis (1986). However, there is still a lack of analytical results for three-dimensional boundary-value problems. In this paper, hence, we study the localization in a slender cylinder composed of an incompressible hyperelastic material subjected to tension, based on an analytical approach to solve the three-dimensional governing equations. We also intend to provide mathematical descriptions for some interesting phenomena as observed in experiments.

Jansen and Shah (1997) conducted careful experiments on concrete cylinders by using the feedback-control method. From two test series, the typical stress–displacement behavior for different height–diameter ratios with normal strength and high strength was obtained. It appears that the pre-peak segment of the stress–displacement curves agrees well with the pre-peak part of the stress–strain curves, but the post-peak segment shows a strong dependence on the geometric size (i.e., the radius–length ratio). More specifically, the longer the specimen is, the steeper the post-peak part of the stress–displacement curves becomes. Also, they found that the width of the localization zone changes with the specimen size. In the experiment by Gopalaratnam and Shah (1985), it was found that the tangent value in the ascending part of the stress–strain curves seemed to be independent of the specimen size but in the post-peak part there was a softening region and no unique stress–strain relation. Schreyer and Chen (1986) studied the softening phenomena analytically based on a one-dimensional model. Their results indicate that if the size of the softening zone is small enough (in a relative sense), the behavior of displacement-prescribed loading is unstable, and the softening curves are steeper than those with a larger size of the softening region. Here, we shall provide the three-dimensional analytical solutions to capture all the localized features mentioned above.

Another purpose of this research is to provide a method judging the onset of failure in a slender cylinder subjected to tension. Here, we use the maximum-distortion-energy theory (the Huber-Hencky-Von Mises theory; see Riley et al., 2007), which depicts there are two portions of the strain energy intensity. One is the portion producing volume change which is ineffective in causing failure by yielding, and the other is that producing the change of shape which is completely responsible for the material failure by yielding.

By constructing the analytical solutions for localizations, it is possible to get the point-wise energy distribution. Then, an expression for the maximum value of the strain energy can be obtained. With the Huber-Hencky-Von Mises theory, we can then establish an analytical criterion for identifying the onset of failure.

Mathematically, to deduce the analytical solutions for localizations in a three-dimensional setting is a very difficult task. One needs to deal with coupled nonlinear partial differential equations together with complicated boundary conditions. Further, the existence of multiple solutions (corresponding to no unique stress–strain relation) makes the problem even harder to solve. Here, the analysis is carried out by a novel method developed earlier (Dai and Huo, 2002; Dai and Fan, 2004; Dai and Cai, 2006), which is capable of treating the bifurcations of nonlinear partial differential equations. Our results yield the analytical forms of the strain and stress fields, total elongation, the potential energy distribution and the strain energy distribution, which are characterized by localization phenomena. In particular, it is found that once the localization is formed its width does not change with the further increase of the total elongation, which is in agreement with the experimental observations. We also provide a description for the snap-through phenomenon.

The remaining parts of the paper are arranged as follows. In Section 2, we formulate the three-dimensional governing equations for the axisymmetric deformations of a circular cylinder. We nondimensionalize them in Section 3 to identify the key small variable and key small parameters. Then, in Section 4, a novel method of coupled series-asymptotic expansions is used to derive the normal form equation of the original system. By the variational principle, in Section 5, we derive the same equation by considering the energy. In Section 6, with the help of the phase plane, we solve the boundary-value problems for a given external axial force and a given elongation, respectively. In Section 7, through an energy analysis, we determine the most preferred configurations and give a description of the snap-through phenomenon. Also, an analytical criterion for identifying

material failure based on the Huber-Hencky-Von Mises theory is discussed. Finally, concluding remarks and future tasks are given in Section 8.

2. Three-dimensional governing equations

We consider the axisymmetric deformations of a slender cylinder subjected to a static axial force at one plane end with the other plane end fixed. The radius of the cylinder is a and the length is l. We take a cylindrical coordinate system, and denote (R,Θ,Z) and (r,θ,z) as the coordinates of a material point of the cylinder in the reference and current configurations, respectively. The radial and axial displacements can be written as:

$$u(R,Z)=r(R,Z)-R,\quad w(R,Z)=z(R,Z)-Z. \tag{1}$$

We suppose that the cylinder is composed of an incompressible hyperelastic material, for which the strain energy density Φ is a function of the first two invariants I_1 and I_2 of the left Cauchy-Green strain tensor, i.e., $\Phi=\Phi(I_1,I_2)$. Moreover the first Piola–Kirchhoff stress tensor $\mathbf{\Sigma}$ is given by

$$\mathbf{\Sigma}^T=\frac{\partial\Phi}{\partial\mathbf{F}}-p\mathbf{F}^{-T}, \tag{2}$$

where $\mathbf{F}$ is the deformation gradient and p is the indeterminate pressure. If the strains are small, it is possible to expand the first Piola–Kirchhoff stress components in terms of the strains up to any order. The expressions for the stress components are very lengthy, and due to the complexity of calculations, we shall only work up to the third-order material nonlinearity. The formula containing terms up to the third-order material nonlinearity has been provided by Fu and Ogden (1999):

$$\Sigma_{ji}=a^1_{jilk}\eta_{kl}+\frac{1}{2}a^2_{jilknm}\eta_{kl}\eta_{mn}+\frac{1}{6}a^3_{jilknmqp}\eta_{kl}\eta_{mn}\eta_{pq}+p_0(\eta_{ji}-\eta_{jk}\eta_{ki}+\eta_{jk}\eta_{kl}\eta_{li})-p^*(\delta_{ji}-\eta_{ji}+\eta_{jk}\eta_{ki})+O(|\eta_{ij}|^4), \tag{3}$$

where

$$\eta=\mathbf{F}-\mathbf{I}=\begin{pmatrix}\frac{\partial u}{\partial R} & 0 & \frac{\partial u}{\partial Z}\\ 0 & \frac{u}{R} & 0\\ \frac{\partial w}{\partial R} & 0 & \frac{\partial w}{\partial Z}\end{pmatrix},$$

p_0 is the pressure value in Eq. (2) corresponding to zero strains, p^* is the incremental pressure, and a^1_{jilk}, a^2_{jilknm}, and $a^3_{jilknmqp}$ are incremental elastic moduli defined by

$$\begin{aligned}&a^1_{jilk}=\frac{\partial^2\Phi}{\partial F_{ij}\partial F_{kl}}|_{F=I},\quad a^2_{jilknm}=\frac{\partial^3\Phi}{\partial F_{ij}\partial F_{kl}\partial F_{mn}}|_{F=I},\\ &a^3_{jilknmqp}=\frac{\partial^4\Phi}{\partial F_{ij}\partial F_{kl}\partial F_{mn}\partial F_{pq}}|_{F=I}.\end{aligned} \tag{4}$$

It can be found that

$$p_0=4\Phi_{01}+2\Phi_{10},$$

where Φ_{01} denotes the first-order partial derivative of Φ with respect to the invariant I_2 at $\mathbf{F}=\mathbf{I}$, and Φ_{10} denotes the first-order partial derivative of Φ with respect to the invariant I_1 at $\mathbf{F}=\mathbf{I}$. In the following derivations, we shall also use Φ_{ij} to denote the i-th order and the j-th order partial derivative of Φ with respect to the invariants I_1 and I_2 at $\mathbf{F}=\mathbf{I}$. All the coefficients in Eq. (4) can be expressed in terms of $\Phi_{10},\Phi_{20},\Phi_{01},\Phi_{02}$, and Φ_{11}, and here for brevity the expressions are omitted.

The equilibrium equations for a static and axisymmetric problem are given by

$$\frac{\partial \Sigma_{zZ}}{\partial Z}+\frac{\partial \Sigma_{rZ}}{\partial R}+\frac{\Sigma_{rZ}}{R}=0, \tag{5}$$

$$\frac{\partial \Sigma_{rR}}{\partial R}+\frac{\partial \Sigma_{zR}}{\partial Z}+\frac{\Sigma_{rR}-\Sigma_{\theta\Theta}}{R}=0. \tag{6}$$

The incompressibility condition yields that

$$\eta_{ii}=\frac{1}{2}\eta_{mn}\eta_{nm}-\frac{1}{2}\eta_{ii}^2-\det(\eta_{mn}). \tag{7}$$

We consider the case where the lateral surface of the cylinder is traction-free, then the stress components Σ_{rR} and Σ_{rZ} should vanish on the lateral surface. Thus, we have the boundary conditions:

$$\Sigma_{rR}|_{R=a}=0, \quad \Sigma_{rZ}|_{R=a}=0. \tag{8}$$

Eqs. (5)–(7) together with Eq. (3) provide three governing equations for three unknowns u, w and p^*. The former two are very complicated nonlinear partial differential equations (PDE's) and the boundary conditions (8) are also complicated nonlinear relations (cf. (11)–(15)). To describe the localization, one needs to study the bifurcation of this complicated system of nonlinear PDE's. As far as we know, there is no available mathematical method. Here, we shall adapt a novel approach involving coupled series-asymptotic expansions to tackle this bifurcation problem. A similar methodology has been developed to study nonlinear waves and phase transitions (Dai and Huo, 2002; Dai and Fan, 2004; Dai and Cai, 2006). First, we shall nondimensionalize this system to identify the relevant small variable and small parameters.

3. Nondimensionalized equations

We introduce the dimensionless quantities through the following scales:

$$s=l^2\tilde{s}, \quad Z=l\tilde{z}, \quad w=h\tilde{w}, \quad v=\frac{h}{l}\tilde{v}, \quad \frac{p^*}{\mu}=\frac{h}{l}\tilde{p}^*, \tag{9}$$

where l is the length of the cylinder, h is the total elongation of the cylinder and μ is the material shear modulus, with a transformation being defined by

$$u=vR, \quad s=R^2. \tag{10}$$

Substituting Eqs. (2), (9) and (10) into Eqs. (5)–(7), we obtain

$$-p_z^*+b_{14}v_z+4b_{10}w_s+b_2w_{zz}+s(b_{14}v_{sz}+4b_{10}w_{ss})+\cdots=0, \tag{11}$$

$$-2p_s^*+8b_2v_s+b_{10}v_{zz}+b_{14}w_{sz}+s4b_2v_{ss}+\cdots=0, \tag{12}$$

$$2v+w_z+2sv_s+\varepsilon[v^2+2vw_z+2s(vv_s-v_zw_s+v_sw_z)]+\varepsilon^2[v^2w_z+2sv(v_sw_z-v_zw_s)]=0, \tag{13}$$

where $\varepsilon=\frac{h}{l}$ is regarded as a small parameter. For convenience, we have replaced $\tilde{s},\tilde{v},\tilde{w},\tilde{z},\tilde{p}^*$ by s,v,w,z,p^* in the nondimensionalized equations. Here and thereafter, a subscript letter is used to represent the corresponding partial derivative (i.e., $v_z=\frac{\partial v}{\partial z}$). The full forms of (11) and (12) are very lengthy and we do not write out the nonlinear terms explicitly for brevity.

Substituting (9) and (10) into the traction-free boundary conditions (8), we have

$$\begin{aligned}
&-p^*+b_{14}v+2b_1w_z+v2b_2v_s+\varepsilon[p^*v+b_{46}v^2+b_{39}vw_z+b_6w_z^2\\
&+v(2p^*v_s+b_{15}vv_s+3b_4v_z^2-2b_{11}v_zw_s+12b_4w_s^2+4b_6v_sw_z)\\
&+v^24b_5v_s^2]+\varepsilon^2[-p^*v^2+3b_{47}v^3+30b_7v^2w_z+b_{16}vw_z^2+4b_8w_z^3\\
&+v(-2p^*(2vv_s+v_zw_s)+b_{22}v^2v_s+7b_9vv_z^2+b_{23}vv_zw_s\\
&+28b_9vw_s^2+72b_{12}vv_sw_z+2b_{19}v_z^2w_z+2b_8v_zw_sw_z+8b_{19}w_s^2w_z\\
&+b_{18}v_sw_z^2)+v^2(-4p^*v_s^2+3b_{31}vv_s^2+4b_{19}v_sv_z^2+8b_{13}v_sv_zw_s\\
&+16b_{19}v_sw_s^2+b_{20}v_s^2w_z)+v^3b_{21}v_s^3]|_{s=v}=0,
\end{aligned} \tag{14}$$

$$
\begin{aligned}
&b_{10}(v_z+2w_s)+\varepsilon[p^*v_z-b_{41}vv_z+2b_{17}vw_s-b_{11}v_zw_z\\
&+12b_4w_sw_z+v(-2b_{11}v_sv_z+24b_4v_sw_s)]+\varepsilon^2[-p^*(vv_z+v_zw_z)\\
&+b_{44}v^2v_z+2b_{16}v^2w_s+b_{30}vv_zw_z+b_{32}vw_sw_z+b_{13}v_zw_z^2\\
&+b_{33}w_sw_z^2+v(-2p^*v_sv_z+b_{23}vv_sv_z-b_3v_z^3+56b_9vv_sw_s\\
&+2b_{11}v_z^2w_s-12b_3v_zw_s^2+16b_5w_s^3+2b_8v_zv_sw_z\\
&+16b_{19}v_sw_sw_z)+v^2(4b_{13}v_s^2v_z+16b_{14}v_s^2w_s)]|_{s=v}=0,
\end{aligned}
\tag{15}
$$

where $v=\frac{a^2}{l^2}$ is a small parameter for a slender cylinder.

Then, Eqs. (11)–(15) compose a new system of complicated nonlinear PDE's with complicated boundary conditions, which is still very difficult to solve exactly. However, it is characterized by a small variable s and two small parameters (ε and v), which permit us to use expansion methods to proceed further.

Remark. The coefficients $b_1, b_2, \cdots$ in Eqs. (11)–(15) can be expressed in terms of $\Phi_{10}, \Phi_{20}, \Phi_{01}, \Phi_{02}$ and Φ_{11}, and for brevity we omit their expressions.

4. Coupled series-asymptotic expansions

We note that s is also a small variable as $0 \leqslant s \leqslant v$. An important feature of the system (11)–(15) is that the unknowns w, v, and p^* become the functions of the variable z, the small variable s and the small parameters ε and v, i.e.,

$$
w=w(z,s;\varepsilon,v),\quad v=v(z,s;\varepsilon,v),\quad p^*=p^*(z,s;\varepsilon,v). \tag{16}
$$

Now, we shall use coupled series-asymptotic expansions to derive the normal form equation of the original nonlinear PDE system. The calculations are very lengthy and can be found on an online report (see http://www.arxiv.org/PS_cache/arxiv/pdf/0711/0711.2924v1.pdf). Here, we just describe the main ideas.

We assume that w, v, p^* have the following Taylor expansions in the neighborhood of the small variable $s=0$:

$$
p^*=P_0(z;\varepsilon,v)+sP_1(z;\varepsilon,v)+s^2P_2(z;\varepsilon,v)+\cdots, \tag{17}
$$

$$
v=V_0(z;\varepsilon,v)+sV_1(z;\varepsilon,v)+s^2V_2(z;\varepsilon,v)+\cdots, \tag{18}
$$

$$
w=W_0(z;\varepsilon,v)+sW_1(z;\varepsilon,v)+s^2W_2(z;\varepsilon,v)+\cdots. \tag{19}
$$

Substituting Eqs. (17)–(19) into Eqs. (11)–(13), the left-hand sides become infinite series in s. All the coefficients of $s^n \quad (n=0,1,2,\ldots)$ should be zero, and as a result, one obtains three sets of infinitely-many equations. Take for consideration the first five equations (coming from the coefficients of s^0 and s^1 from the axial equilibrium Eq. (11), the coefficients of s^0 from the radial equilibrium Eq. (12), and the coefficients of s^0 and s^1 from the incompressibility condition (13)). They contain seven unknowns: $P_0, P_1, V_0, V_1, W_0, W_1$ and W_2. To obtain a closed-system, we further substitute Eqs. (17)–(19) into the traction-free boundary conditions (14) and (15). Then by neglecting the terms higher than $O(v\varepsilon, \varepsilon^2)$, two more equations for $P_0, P_1, V_0, V_1, W_0, W_1$ and W_2 are obtained. Therefore, we have seven nonlinear ODE's for these seven unknowns. However, these seven equations are still very complicated and it is very difficult to analyze them directly. By further using asymptotic expansions in the small parameter ε, it is possible to express the other six unknowns in terms W_{0z}. Then, we obtain a single equation for W_{0z}. It turns out that equation can be integrated once to give

$$
3b_{10}W_{0z}-\varepsilon\frac{b_{100}}{2}W_{0z}^2+\varepsilon^2b_{110}W_{0z}^3-\frac{3}{4}vb_{10}W_{0zzz}+v\varepsilon b_{35}(W_{0zz}^2+2W_{0z}W_{0zzz})=C, \tag{20}
$$

where C is an integration constant.

To find the physical meaning of C, we consider the resultant force T acting on the material cross section that is planar and perpendicular to the cylinder axis in the reference configuration, and the formula is

$$T = \int_0^{2\pi} \int_0^a \Sigma_{zZ} R \mathrm{d}R\mathrm{d}\Theta. \tag{21}$$

After expressing Σ_{zZ} in terms of W_{0z} by using the results obtained above, the integration can be carried out, and as a result we find that

$$T = 8\pi a^2 \mu\varepsilon\left(3b_{10}W_{0z} - \varepsilon\frac{b_{100}}{2}W_{0z}^2 + \varepsilon^2 b_{110}W_{0z}^3 - \frac{3}{4}\nu b_{10}W_{0zzz} + \nu\varepsilon b_{35}(W_{0zz}^2 + 2W_{0z}W_{0zzz})\right). \tag{22}$$

Comparing Eqs. (20) and (22), we have $C = \frac{T}{8\pi a^2\mu\varepsilon}$. Thus, we can rewrite Eq. (22) as

$$3b_{10}\varepsilon W_{0z} - \frac{b_{100}}{2}(\varepsilon W_{0z})^2 + b_{110}(\varepsilon W_{0z})^3 - \frac{3}{4}\nu\varepsilon b_{10}W_{0zzz} + \nu\varepsilon^2 b_{35}(W_{0zz}^2 + 2W_{0z}W_{0zzz}) = \frac{T}{8\pi a^2\mu}. \tag{23}$$

If we retain the original dimensional variable and let $V = W_{0Z} = \varepsilon W_{0z}$, we have

$$V + D_1V^2 + D_2V^3 + a^2\left(-\frac{1}{4}V_{ZZ} + D_3V_Z^2 + 2D_3VV_{ZZ}\right) = \gamma, \tag{24}$$

where

$$D_1 = -\frac{b_{100}}{6b_{10}}, \quad D_2 = \frac{b_{110}}{3b_{10}}, \quad D_3 = \frac{b_{35}}{3b_{10}}, \quad \gamma = \frac{T}{24b_{10}\pi a^2\mu}. \tag{25}$$

Since Eq. (24) is derived from the three-dimensional field equations, once its solution is found, the three-dimensional strain and stress fields can also be found. Also, it contains all the required terms to yield the leading-order behavior of the original system. Therefore, we refer Eq. (24) as the normal form equation of the system of nonlinear PDE's (11)–(13) together with boundary conditions (14) and (15) under a given axial resultant.

5. The Euler–Lagrange equation

It is also possible to deduce the equation for $V = \varepsilon W_{0z}$ by considering the total potential energy and then using the variational principle. By using the expansions obtained in Section 4, we can express the strain energy in terms of W_{0z}, and the result is

$$\begin{aligned}\Phi = {} & \varepsilon^2\mu(6b_{10}W_{0z}^2 - \frac{2}{3}\varepsilon b_{100}W_{0z}^3 + \varepsilon^2 b_{110}W_{0z}^4) \\ & + s\varepsilon^2\mu\left[\frac{81}{64}b_{10}W_{0zz}^2 - \frac{15}{64}b_{10}W_{0z}W_{0zzz} + \varepsilon(F_1W_{0z}W_{0zz}^2 + F_2W_{0z}^2W_{0zzz})\right].\end{aligned} \tag{26}$$

The stored energy per unit length is given by

$$\Psi = \int_0^a \int_0^{2\pi} \Phi R \mathrm{d}R\mathrm{d}\Theta. \tag{27}$$

Substituting Eq. (26) into Eq. (27) and carrying out the integration, we obtain the average stored energy over a cross section:

$$\begin{aligned}\widetilde{\Psi} = \frac{\Psi}{\pi a^2} = {} & 2\varepsilon^2\mu\left(6b_{10}W_{0z}^2 - \frac{2}{3}\varepsilon b_{100}W_{0z}^3 + \varepsilon^2 b_{110}W_{0z}^4\right) \\ & + 2a^2\varepsilon^2\mu\left[\frac{81}{64}b_{10}W_{0zz}^2 - \frac{15}{64}b_{10}W_{0z}W_{0zzz} + \varepsilon(F_1W_{0z}W_{0zz}^2 + F_2W_{0z}^2W_{0zzz})\right].\end{aligned} \tag{28}$$

Letting $V = W_{0Z} = \varepsilon W_{0z}$, we can further rewrite the above equation as

$$\widetilde{\Psi} = E\left[\frac{1}{2}V^2 + \frac{1}{3}D_1V^3 + \frac{1}{4}D_2V^4 + a^2\left(\frac{27}{256}V_Z^2 - \frac{5}{256}VV_{ZZ} + F_1VV_Z^2 + F_2V^2V_{ZZ}\right)\right], \tag{29}$$

where $E = 24\mu b_{10}$ is the Young's modulus, F_1 and F_2 are constants related to material parameters.

The total potential energy for a force-controlled problem is given by

$$L = \pi a^2\left(\int_0^1 \widetilde{\Psi}\mathrm{d}Z - E\int_0^1 \gamma V \mathrm{d}Z\right)$$
$$= \pi a^2 E\int_0^1 \left(-\gamma V + \frac{1}{2}V^2 + \frac{1}{3}D_1V^3 + \frac{1}{4}D_2V^4 + a^2\left(\frac{27}{256}V_Z^2 - \frac{5}{256}VV_{ZZ} + F_1VV_Z^2 + F_2V^2V_{ZZ}\right)\right)\mathrm{d}Z. \quad (30)$$

By the variational principle, we have the following Euler-Lagrange equation:

$$\frac{\partial L}{\partial V} - \frac{\mathrm{d}}{\mathrm{d}Z}\frac{\partial L}{\partial V_Z} + \frac{\mathrm{d}^2}{\mathrm{d}Z^2}\frac{\partial L}{\partial V_{ZZ}} = 0, \quad (31)$$

which yields that

$$V + D_1V^2 + D_2V^3 + a^2\left(D_3V_Z^2 - \frac{1}{4}V_{ZZ} + 2D_3VV_{ZZ}\right) = \gamma, \quad (32)$$

which is just Eq. (24). This shows that the normal form Eq. (24) obeys the variational principle for energy.

If we multiply V_Z to both sides of Eq. (32), it can be integrated once to yield that

$$\frac{1}{2}V^2 + \frac{1}{3}D_1V^3 + \frac{1}{4}D_2V^4 - a^2\left(\frac{1}{8}V_Z^2 - D_3VV_Z^2\right) = \gamma V + K, \quad (33)$$

where K is an integration constant.

In the following section, we shall discuss the solutions for two boundary-value problems based on Eqs. (32) and (33), and reveal their main characteristics.

6. Solutions for two boundary-value problems

We rewrite Eq. (32) as a first-order system as follows:

$$V_Z = y,$$
$$y_Z = \frac{-\gamma + V + D_1V^2 + D_2V^3 + a^2D_3y^2}{a^2(\frac{1}{4} - 2D_3V)}. \quad (34)$$

Without loss of generality, we take the length l of the cylinder to be 1, then a is equivalent to the radius–length ratio. We suppose that the two plane ends of the cylinder are attached to rigid bodies. Then we have

$$z = 0 \text{ (or constant)}, \quad \text{at } Z = 0, 1, \quad (35)$$

and

$$r = R, \quad \text{at } Z = 0, 1. \quad (36)$$

We point out that although Eq. (32) is one-dimensional, it is derived from the three-dimensional governing equations, and as a result we can also derive the proper boundary conditions by considering the condition in the other (radial) dimension such as Eq. (36). If one directly introduces a one-dimensional model (say, using a gradient theory), such an option is not available. So, this is another advantage of Eq. (32). From Eqs. (35) and (36), we have

$$w_R = 0(\text{i.e.}, z_R = 0), \text{ and } u_R = 0 \text{ (i.e.}, r_R = 1) \quad \text{at } Z = 0, 1. \quad (37)$$

Substituting Eq. (37) into Eq. (7) and integrating with respect to R once, we obtain

$$w_z = 0, \quad \text{at } Z = 0, 1. \quad (38)$$

Thus, the proper boundary conditions for Eq. (32) are

$$V = 0, \quad \text{at } Z = 0, 1. \quad (39)$$

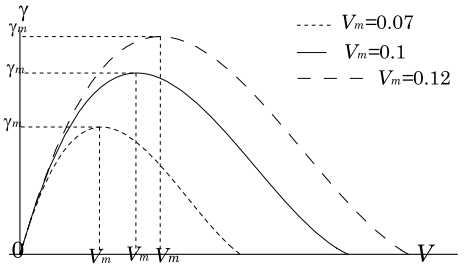

Fig. 1. $\gamma - V$ plot.

To solve this boundary-value problem of the first-order system (34) under Eq. (39), we shall conduct a phase-plane analysis with the engineering stress as the bifurcation parameter. The critical points of this system is given by

$$y = 0, \quad \text{and } V + D_1 V^2 + D_2 V^3 = \gamma. \tag{40}$$

Here, we shall consider a class of strain energy functions $\Phi(I_1, I_2)$ such that the $\gamma - V$ plot based on Eq. $(40)_2$ has one peak, and this requires that

$$D_1 < 0, \quad D_2 > 0, \quad D_1^2 > 4D_2.$$

The $\gamma - V$ curves corresponding to Eq. $(40)_2$ are plotted in Fig. 1.

In this figure, γ_m is the local maximum of the stress and V_m is the corresponding strain value, and they are given by $V_m = -\frac{D_1+\sqrt{D_1^2-3D_2}}{3D_2}$, $\gamma_m = -\frac{2D_1^3+2(D_1^2-3D_2)^{3/2}-9D_1D_2}{27D_2^2}$. When we take $D_1 = -9.45, D_2 = 22$ and $D_3 = -2$, V_m =0.07; when we take D_1 =−6.65, $D_2 = 11$ and $D_3 = -2$, $V_m = 0.1$; when we take $D_1 = -5.53, D_2 = 7.6$ and $D_3 = -2$, $V_m = 0.12$. The three curves in Fig. 1 correspond to these values of D_1, D_2 and D_3, respectively.In the following discussions we consider the tension case so that $\gamma > 0$. Similar analysis can be made for the compression case, which will not be discussed here. Eq. (33) can be rewritten as

$$V_Z^2 = \frac{-K - \gamma V + \frac{1}{2}V^2 + \frac{1}{3}D_1V^3 + \frac{1}{4}D_2V^4}{a^2\left(\frac{1}{8} - D_3V\right)}. \tag{41}$$

In this paper, we consider the case of $D_3 \leqslant 0$. New phenomena can arise for $D_3 > 0$ and the results will be reported elsewhere. For the present case, the phase plane always has a saddle point and a center point as γ varies, which is shown in Fig. 2.

In this figure, $(V_s, 0)$ and $(V_c, 0)$ are a saddle point and a center point, respectively. There are two solutions for the same stress γ, which are represented by the curve 1 and the curve 2 in Fig. 2, respectively. For curve 1, the right hand of Eq. (41) have four real roots, which we label in an increasing order by α_1, g_1, g_2 and α_2. We note that the smallest root α_1 is smaller than V_s. So, from Eq. (41) we obtain the following expression:

$$V_Z = \pm\frac{\sqrt{2D_2}}{a\sqrt{1-8D_3V}}\sqrt{(V-\alpha_1)(V-g_1)(V-g_2)(V-\alpha_2)}. \tag{42}$$

Then, an integration leads to

$$Z = \begin{cases} \frac{1}{2} - \frac{a}{\sqrt{2D_2}}\int_V^{\alpha_1}\sqrt{\frac{1-8D_3t}{(t-\alpha_1)(t-g_1)(t-g_2)(t-\alpha_2)}}\mathrm{d}t, & Z \in \left[0, \frac{1}{2}\right] \\ \frac{1}{2} + \frac{a}{\sqrt{2D_2}}\int_V^{\alpha_1}\sqrt{\frac{1-8D_3t}{(t-\alpha_1)(t-g_1)(t-g_2)(t-\alpha_2)}}\mathrm{d}t, & Z \in \left[\frac{1}{2}, 1\right]. \end{cases} \tag{43}$$

By Eq. (39), α_1 can be determined by the following two equations:

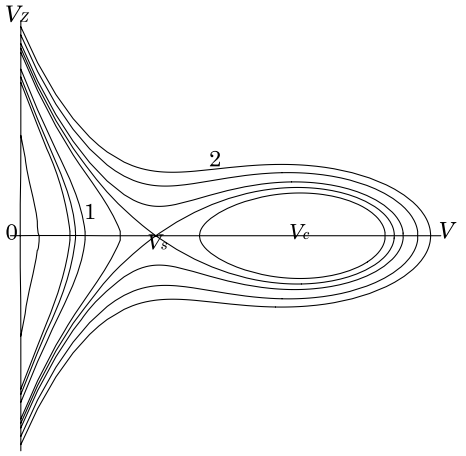

Fig. 2. The phase plane.

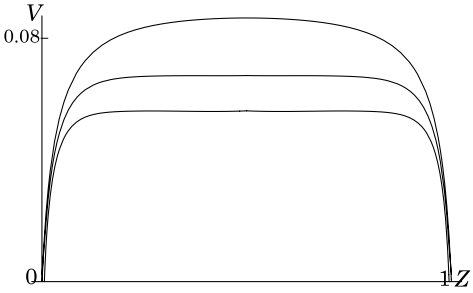

Fig. 3. V–Z plot. From bottom to top, $\gamma = 0.037825, \gamma = 0.04005, \gamma = 0.0445$.

$$\frac{1}{2} = a\sqrt{-D_3}\int_0^{\alpha_1}\sqrt{\frac{t-\frac{1}{8D_3}}{-K-\gamma t+\frac{1}{2}t^2+\frac{1}{3}D_1t^3+\frac{1}{4}D_2t^4}}\mathrm{d}t, \tag{44}$$

$$K = -\gamma\alpha_1+\frac{1}{2}\alpha_1^2+\frac{1}{3}D_1\alpha_1^3+\frac{1}{4}D_2\alpha_1^4. \tag{45}$$

Once α_1 is found, the solution corresponding to curve 1 can be obtained from Eq. (43) by numerical integration. In Fig. 3, we have plotted the solution curves for three different values of the engineering stress γ.

From this figure, we find there is nearly a uniform extension in the middle part, but there are two boundary-layer regions near the two ends of the cylinder in order to satisfy the boundary conditions.

There is another solution which is represented by curve 2 in Fig. 2, and we denote the point as α at which $V_Z = 0$. Then, Eq. (41) can be rewritten as

$$V_Z = \pm\frac{\sqrt{2D_2}}{a\sqrt{1-8D_3V}}\sqrt{(\alpha-V)(\beta-V)[(V-m)^2+n^2]}, \tag{46}$$

where β is another real root of the right-hand of Eq. (41), and $m = -\frac{4D_1+3(\alpha+\beta)D_2}{6D_2}$ and $n^2 = \frac{-16D_1^2+24(\alpha+\beta)D_1D_2+9D_2(8+(3\alpha^2+2\alpha\beta+3\beta^2)D_2)}{36D_2^2}$. Then, we obtain

$$Z = \begin{cases}\frac{1}{2}-\frac{a}{\sqrt{2D_2}}\int_V^{\alpha}\sqrt{\frac{1-8D_3t}{(\alpha-t)(\beta-t)[(t-m)^2+n^2]}}\mathrm{d}t, & Z\in\left[0,\frac{1}{2}\right]\\ \frac{1}{2}+\frac{a}{\sqrt{2D_2}}\int_V^{\alpha}\sqrt{\frac{1-8D_3t}{(\alpha-t)(\beta-t)[(t-m)^2+n^2]}}\mathrm{d}t, & Z\in\left[\frac{1}{2},1\right].\end{cases} \tag{47}$$

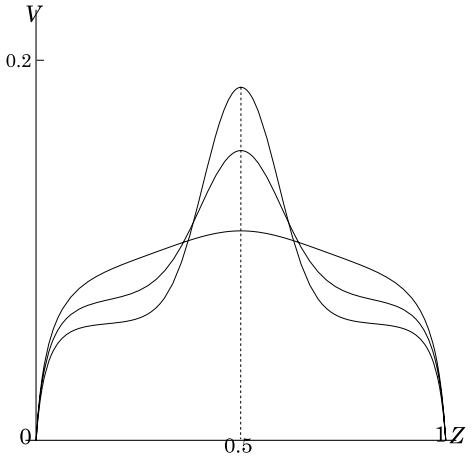

Fig. 4. V–Z plot. From top to bottom (along the dashed line): $\gamma = 0.037825, \gamma = 0.04005, \gamma = 0.0445$.

By Eq. (39), α can be determined by

$$\frac{1}{2} = a\sqrt{-D_3}\int_0^{\alpha}\sqrt{\frac{t-\frac{1}{8D_3}}{-K-\gamma t+\frac{1}{2}t^2+\frac{1}{3}D_1t^3+\frac{1}{4}D_2t^4}}\mathrm{d}t, \tag{48}$$

$$K = -\gamma\alpha+\frac{1}{2}\alpha^2+\frac{1}{3}D_1\alpha^3+\frac{1}{4}D_2\alpha^4. \tag{49}$$

By numerical integration, we can get α from Eqs. (48) and (49). Then the solution corresponding to curve 2 can be obtained from (47) by numerical integration. In Fig. 4, we have plotted the solution curves for three different values of the engineering stress γ.

In this figure, there is a sharp-change region in the middle of the slender cylinder, that represents the localization and energy concentration. Moreover, the tip is sharper when the engineering stress is smaller.

From Eq. (47), one can see that the localization solution depends on Z through the form $\left(Z-\frac{1}{2}\right)/a$, and this implies that the localization zone width is proportional to a for a fixed length; cf. Jansen and Shah (1997).

The solutions obtained above are for a given γ. To obtain the solutions for a displacement-controlled problem, we follow the idea in Dai and Bi (2006). For that purpose, we need to get the engineering stress–strain curve.

The total elongation is given by

$$W_0|_{Z=1} - W_0|_{Z=0} = \int_0^1 V\mathrm{d}Z = \Delta, \tag{50}$$

where the total elongation Δ is actually the engineering strain since we have taken the length of the cylinder to be 1. According to the symmetric phase plane and Eqs. (43) and (47), V is a function of Z, so we can get the total elongation by numerical integrations. In Fig. 5, we have plotted the curves between the total elongation Δ and the engineering stress γ with different material coefficients corresponding to Fig. 1.

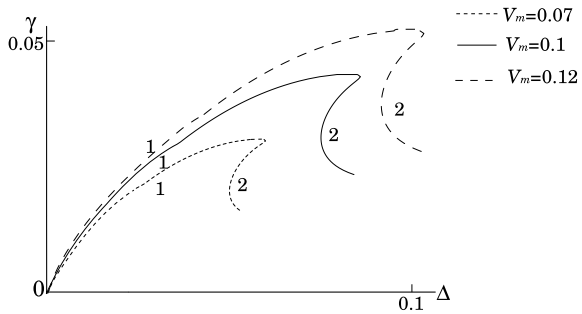

Fig. 5. The engineering stress–strain curves.

Segment 1 corresponds to the solution given by Eq. (43) (we call it as Solution 1), and segment 2 corresponds to the solution given by Eq. (47) (we call it as Solution 2). For a displacement-controlled problem (i.e., given Δ), from Fig. 5, we can get the corresponding γ value(s), then the solution(s) is given by Eq. (43) or Eq. (47).

From Eqs. (1), (9), (10), (18) and (19), we can get the shapes of the cylinder corresponding to Eq. (47) under different material coefficients for a given Δ, which are shown in Fig. 6, where we take $D_3 = -0.5, F_2 = -4$, and $a = 0.04$.

In this figure, the width δ of the localization is defined as $1 - 2\overline{Z}$, where $\overline{Z}$ is the point where the rate of the slope of the surface radial displacement is the maximum. From the above figure, one can see that for different material coefficients the localization widths are different and the localization width is almost the same for the same material coefficients with different loads of engineering stress. That is to say, for different materials the localizations have different widths, but for the same material, the localization width is almost uniform during the loading process.

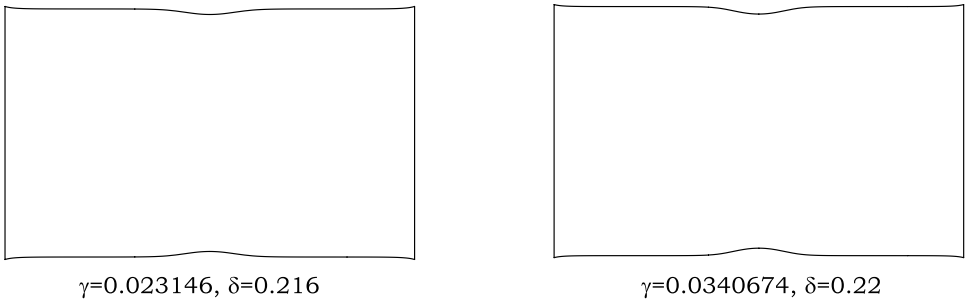

(a) Δ=0.0740121 for Vm=0.07

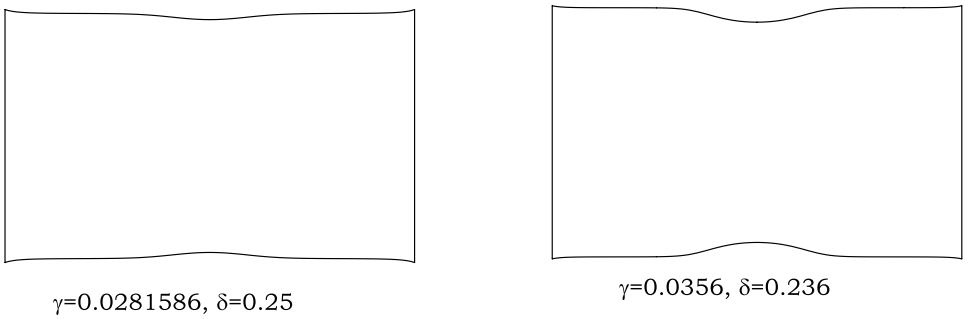

(b) Δ=0.0811761 for Vm=0.1

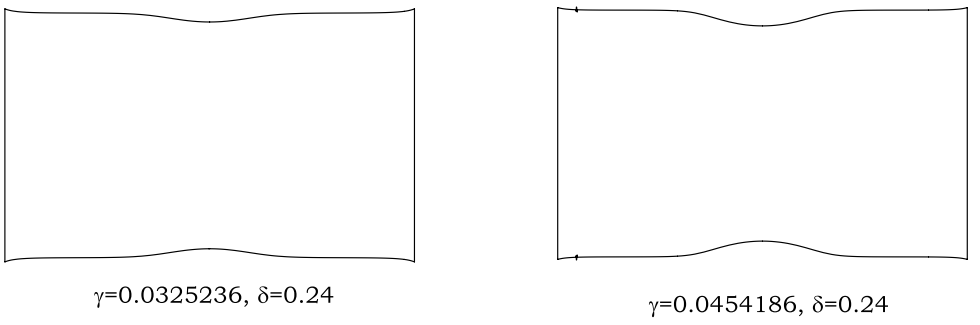

(c) Δ=0.10055 for Vm=0.12

Fig. 6. Shapes of the cylinder corresponding to the localization solutions and the comparison of the localization widths δ.

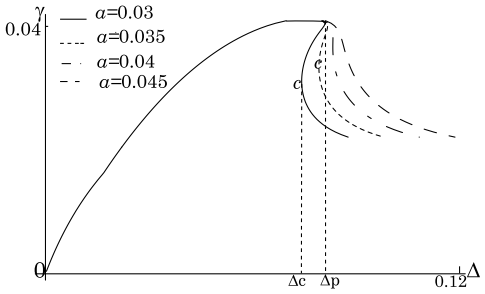

Fig. 7. The engineering stress–strain curves for different a.

Here and thereafter, we fix the material constants to be $D_1 = -6.65, D_2 = 11$, and $D_3 = -2$. By the same way, we can get the relations between the total elongation Δ and the engineering stress γ with different radius–length ratios, which are shown in Fig. 7.

In this figure, we observe that there is a snap-back for a relatively small value of a. We also see that the point c (across which there are multiple values for γ for a given Δ) moves up and toward right as the value of a increases. For example, when $a = 0.03, \quad \gamma_c = 0.0339$, and when $a = 0.04, \quad \gamma_c = 0.0399$. The post-peak curves show very significant changes. There is no unique stress–displacement relationship in the post-peak region. The thinner the specimen is, the steeper the curve becomes, which is in agreement with the experimental results by Jansen and Shah (1997). From this figure, we see that for $a = 0.03$, unstable behavior is predicted for a displacement-controlled loading whereas larger values of a yield results that are stable. Similar conclusions follow from the examples given by Schreyer and Chen (1986).

As to $a = 0.045$, there is a stable relation between the total elongation Δ and the engineering stress γ, which is in agreement with the experiment result by Gopalaratnam and Shah (1985), who conducted tensile tests on concrete under carefully controlled loading conditions and with refined measuring techniques.

We note that for a displacement-controlled problem, after the elongation $\Delta \geqslant \Delta_c$ (cf. Fig. 7) there are bifurcations from one solution to two solutions (at $\Delta = \Delta_c$), to three solutions ($\Delta_c < \Delta < \Delta_p$), to two solutions ($\Delta = \Delta_p$), and to one solution ($\Delta > \Delta_p$). The shapes of the cylinder corresponding to these solutions are shown in Fig. 8 for $F_2 = -4$, and $a = 0.03$.

The above figure also manifests that the middle of the cylinder becomes thinner than the two ends as we pull the slender cylinder. The middle part is thinner as the engineering stress decreases for a given Δ, which agrees well with the experimental results.

7. Energy analysis and failure criterion

As discussed in the previous section, for a relatively small a, there are multiple solutions for $\Delta \geqslant \Delta_c$. Of course, in reality only one solution can be observed at one instant. In this section, we shall further consider the energy values for these solutions to deduce which one is most preferred.

From Eq. (33), we have

$$V_Z^2 = \frac{2(12K + 12\gamma V - 6V^2 - 4D_1V^3 - 3D_2V^4)}{3a^2(-1 + 8D_3V)}. \tag{51}$$

Substituting Eq. (51) into Eq. (32), we obtain

$$V_{ZZ} = -\frac{4}{3(-1 + 8D_3V)^2}(3\gamma + 24KD_3 - 3V - 3D_1V^2 - 3D_2V^3 + 12D_3V^2 + 16D_1D_3V^3 + 18D_2D_3V^4). \tag{52}$$

Then by using Eq. (30), we can express the potential energy (for a given γ) in terms of V (scaled by $\pi a^2 E$):

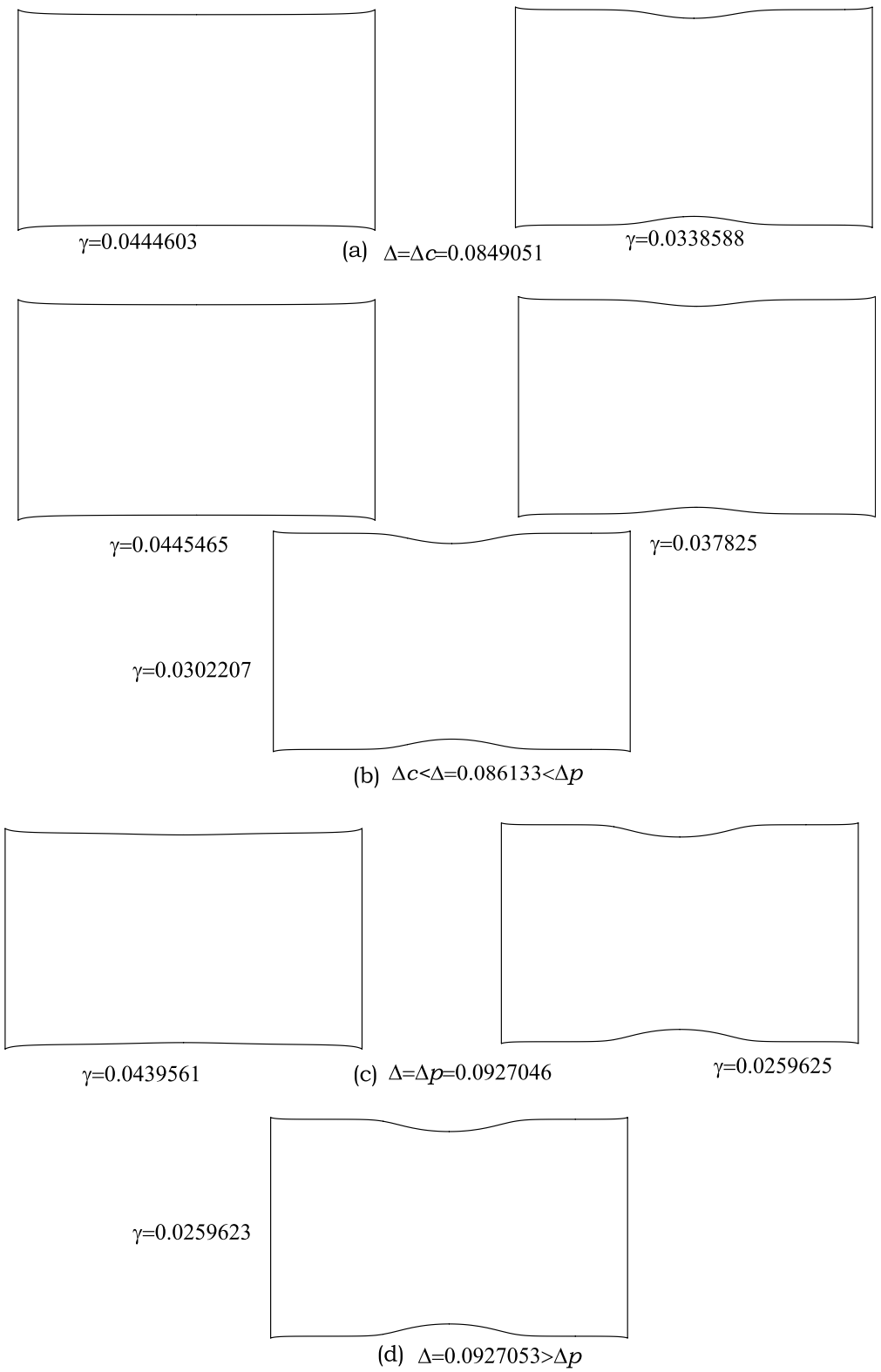

Fig. 8. The shapes of the cylinder under different elongations.

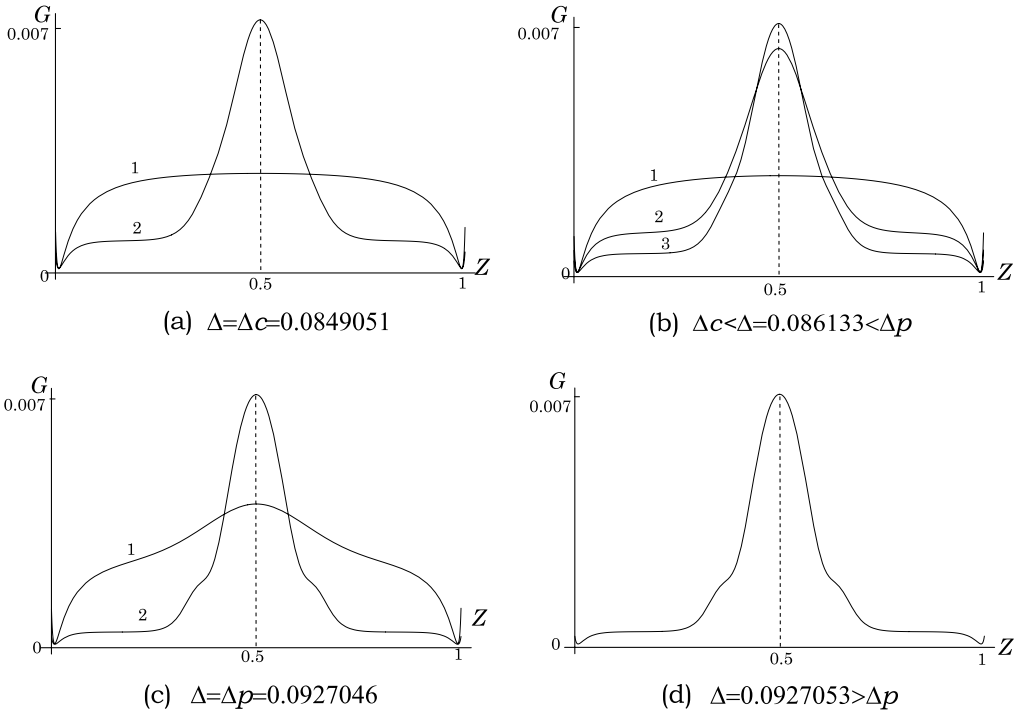

Fig. 9. The stored energy distribution curves for different elongations.

$$
\begin{aligned}
P = & -\frac{1}{384(-1+8D_3V)^2}(2D_1V^3(-118+15a^2-8192D_3^2V^2-256(4+3a^2)F_2V \\
& +16D_3V(123-5a^2+256(2+a^2)F_2V))+3(D_2V^4(-59+10a^2-4096D_3^2V^2-512(1+a^2)F_2V \\
& +4D_3V(246-15a^2+256(4+3a^2)F_2V))+2(54K-59V^2+5a^2V^2+118\gamma V-5a^2\gamma V \\
& +4096V^2(K-V(V-2\gamma))D_3^2+256V(4K+V(-(2+a^2)V+(4+a^2)\gamma))F_2+4D_3V(-2(118+5a^2)K \\
& +V(246V-5a^2V-492\gamma)+256V(2(-4+a^2)K+V((4+a^2)V-8\gamma))F_2)))).
\end{aligned}
\tag{53}
$$

The stored energy is given by

$$
G = P + \gamma V. \tag{54}
$$

Then from Eqs. (44), (47), (53) and (54), one can calculate the energy distributions for a given elongation. The stored energy curves corresponding to those values of Δ in Fig. 8 are plotted in Fig. 9. In this figure, labels 1, 2 and 3 correspond to different values of γ (in a decreasing order).

In Fig. 9(a), the total stored energy values for curve 1 and curve 2 are respectively $G_1^t = 0.00241013$ and $G_2^t = 0.00206265$. Thus for a displacement-controlled problem, as $G_2^t < G_1^t$, the shape in the right of Fig. 8(a) represents a preferred configuration, and at $\Delta = \Delta_c$ there could be a bifurcation from Solution 1 to Solution 2 (a localization solution). Correspondingly, there is a snap-through in the engineering stress–strain curve at $\Delta = \Delta_c$.

In Fig. 9(b), the total stored energy values for curve 1, curve 2 and curve 3 are respectively $G_1^t = 0.00247747$, $G_2^t = 0.00230487$ and $G_3^t = 0.00186959$. For a displacement-controlled problem, as G_3^t is the smallest, the shape in the bottom of Fig. 8(b) represents a preferred configuration.

In Fig. 9(c), the total stored energy value for curve 1 and curve 2 are respectively $G_1^t = 0.00275441$ and $G_2^t = 0.00170114$. For a displacement-controlled problem, as $G_2^t < G_1^t$, the shape in the right of Fig. 8(c) represents a preferred configuration.

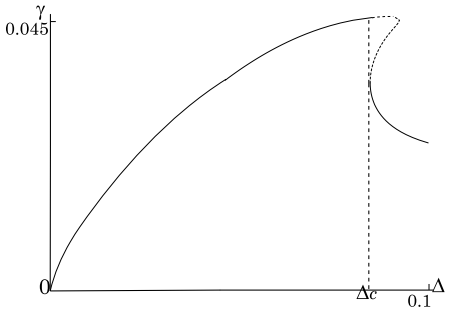

Fig. 10. The engineering stress–strain curve.

In Fig. 10, we have plotted the engineering stress–strain curve corresponding to the preferred configuration for a displacement-controlled problem. We see that a snap-through takes place at $\Delta = \Delta_c$, which leads to the localization (as represented by Solution 2).

Once the localization happens, there is a high concentration of energy around the middle of the cylinder. It is known that if the strain energy density reaches a critical value there will be the material failure. The analytical results obtained here can be used to calculate the stored energy at any material point. The largest energy value is attained at $(R, Z) = (a, \frac{1}{2})$ at which $V = \alpha$ (cf. Eqs. (47)–(49)). From Eqs. (26), (51) and (52), we can express the energy value at this point in terms of α, and the result is

$$\begin{aligned} G_m = & -\frac{1}{384(-1+8D_3\alpha)^2}(2D_1\alpha^3(-118+15a^2-8192D_3^2\alpha^2-256(4+3a^2)F_2\alpha \\ & +16D_3\alpha(123-5a^2+256(2+a^2)F_2\alpha))+3(D_2\alpha^4(-59+10a^2-4096D_3^2\alpha^2-512(1+a^2)F_2\alpha \\ & +4D_3\alpha(246-15a^2+256(4+3a^2)F_2\alpha))+2(54K-59\alpha^2+5a^2\alpha^2+118\gamma\alpha-5a^2\gamma\alpha \\ & +4096\alpha^2(K-\alpha(\alpha-2\gamma))D_3^2+256\alpha(4K+\alpha(-(2+a^2)\alpha+(4+a^2)\gamma))F_2+4D_3\alpha(-2(118+5a^2)K \\ & +\alpha(246\alpha-5a^2\alpha-492\gamma)+256\alpha(2(-4+a^2)K+\alpha((4+a^2)\alpha-8\gamma))F_2)))+\gamma\alpha. \end{aligned} \tag{55}$$

The values of G_m corresponding to those values of Δ (in an increasing order) in Fig. 8 for preferred configurations are respectively $G_m = 0.00722628$, $G_m = 0.00742384$, $G_m = 0.00742989$, and $G_m = 0.00742989$.

Based on the maximum-distortion-energy theory (the Huber-Hencky-Von Mises theory; see Riley et al., 2007), there are two portions of the strain energy intensity: one for volume change and the other for shape change. In the present work, we consider an incompressible material, so there is no strain energy intensity corresponding to the volume change. Then the strain energy is only due to distortion. On the other hand, the strain energy intensity attains its maximum value at the material point $\left(a, \frac{1}{2}\right)$. Thus, we can give the failure criterion

$$G_m = G_f, \tag{56}$$

where G_f is the failure value of the strain energy intensity for a given material. Fracture will occur whenever the energy by Eq. (56) exceeds the limiting value G_f.

8. Concluding remarks and future tasks

To study the localization phenomenon, a phenomenological approach is employed to formulate a three-dimensional boundary value problem with an incompressible hyperelastic constitutive law. A coupled series-asymptotic expansion procedure is developed to solve the nondimensionalized system of governing differential equations with given boundary data for a slender cylinder subjected to axial tension. With the assumptions appropriate for the slender cylinder, analytical solutions have been obtained for the axisymmetric boundary value problem, which demonstrate the essential features of localization problems and are consistent with the experimental data available. Specifically, the width of localization zone depends on the material parameters, and it remains almost unchanged for the same material in the post-peak regime. Also, the

snap-back and snap-through phenomena could be predicted with the analytical approach, and a preferred configuration in the post-peak regime could be identified via an energy analysis. Due to the lack of three-dimensional analytical results available in the open literature, the analytical work presented in this paper could complement the analytical, experimental and numerical efforts made by the research community for the localization problems over the last several decades.

As indicated by Buehler et al. (2003), the hyperelasticity is crucial for understanding and predicting the dynamics of brittle fracture. Especially, the effect of hyperelasticity is important for understanding the failure evolution in nanoscale materials. Since localization identifies the onset of material failure, future work will focus on the identification of the parameters proposed in the current phenomenological model, and on the linkage between the continuum and fracture mechanics approaches, via multiscale analysis.

Acknowledgements

The work described in this paper is supported by two grants from CityU (Project Nos: 7002107 and 7001861).

References

Aifantis, E.C., 1984. On the microstructural origin of certain inelastic models. J. Eng. Mater. Technol. 106, 326–330.
Arthur, P.B., Richard, J.S., 2002. Advanced mechanics of materials. Wiley, New York.
Buehler, M., Abraham, F.F., Gao, H., 2003. Hyper-elasticity governs dynamic fracture at a critical length scale. Nature 426, 141–146.
Chen, Z., Schreyer, H.L., 1994. On nonlocal damage models for interface problem. Int. J. Solids Struct. 31, 1241–1261.
Chen, Z., Sulsky, D., 1995. A partitioned-modeling approach with moving jump conditions for localization. Int. J. Solids Struct. 32, 1893–1905.
Dai, H.H., Bi, Q., 2006. On constructing the unique solution for the necking in a hyper-elastic rod. J. Elasticity 82, 215–241.
Dai, H.H., Cai, Z.X., 2006. Phase transitions in a slender cylinder composed of an incompressible elastic material. I. Asymptotic model equation. Proc. R. Soc. Lond. Ser. A Math. Phys. Eng. Sci. 462, 75–95.
Dai, H.H., Fan, X.J., 2004. Asymptotically approximate model equations for weakly nonlinear long waves in compressible elastic rods and their comparisons with other simplified model equations. Math. Mech. Solids 9, 61–79.
Dai, H.H., Huo, Y., 2002. Asymptotically approximate model equations for nonlinear dispersive waves in incompressible elastic rods. Acta Mech. 157, 97–112.
Fu, Y.B., Ogden, R.W., 1999. Nonlinear stability analysis of pre-stressed elastic bodies. Continuum Mech. Thermodyn. 11, 141–172.
Gopalaratnam, V.S., Shah, S.P., 1985. Softening response of plain concrete in direct tension. J. Am. Concrete Inst. 82, 310–323.
Jansen, D.C., Shah, S.P., 1997. Effect of length on compressive strain softening of concrete. J. Eng. Mech. 123, 25–35.
Riley, W.F., Sturges, L.D., Morris, D.H., 2007. Mechanics of materials. John Wiley & Sons, Inc..
Schreyer, H.L., Chen, Z., 1986. One-dimensional softening with localization. J. Appl. Mech. 53, 791–797.
Triantafyllidis, N., Aifantis, E.C., 1986. A gradient approach to localization of deformation. I. Hyper-elastic materials. J. Elasticity 16, 225–237.